Proceedings of the European Control Conference 2007
Kos, Greece, July 2-5, 2007

Minimum Fuel Techniques for a Space Robot Simulator with a Reaction Wheel and PWM Thrusters

Evangelos Papadopoulos, Ioannis K. Kaliakatsos, and Dimitrios Psarros

Abstract— **Space simulators offer engineers great advantages on studying space-related dynamic behavior without actually having to travel into space. They can test various control and design strategies, leading to close-to-optimal spacecraft missions. In this paper, an air-bearing planar space simulator developed for the experimental study of space robots on orbit is briefly presented. To achieve proportional control of 2-way on-off solenoid valves used for robot propulsion, a voltage PWM actuation is employed. The resulting thrust is analyzed, nonlinear valve effects are identified, and techniques tackling their shortcomings are proposed. The experimentally obtained thruster behavior is used to address a minimum fuel nozzle consumption problem during point-to-point robot motions. A comparison between the thruster-only propulsion method with one which includes a reaction wheel follows. A control algorithm for the simultaneous employment of thrusters and reaction wheel is presented. It is found that under certain assumptions, the use of a reaction wheel further minimizes fuel consumption, increasing the useful life of a space robot.**

I. Introduction

SPACE simulators are being developed worldwide by institutions and universities, in an effort to emulate on earth the space conditions, [5], [8]. It is preferable to run experiments on earth by utilizing space simulators, since the cost of a potential space mission is remarkable. On the other hand, safety reasons and technical requirements impose restrictions on astronauts and equipment, which need to be addressed before a real mission is planned.

There are several setups that are currently being used, in order to artificially bring forth conditions of weightlessness necessary for space simulators, [5]. These include the planar air-bearing simulators, suspension systems, underwater test facilities, or even parabolic flight. Each of the above has its pros and cons, related with the simulator's capability of allowing 3D motion, long-term experiments, and innovation in design. It is worth noticing that in some cases, the results obtained by the simulator cannot be directly applied to real-life space missions, since perturbations are introduced by the simulator's overall design which cannot be compensated neither analytically nor experimentally (for example, water inertia in underwater test facilities).

Air-bearing simulators are being used for spacecraft attitude determination, control hardware verification and software development for more than 40 years, [8]. They are the preferred technology for ground-based research in spacecraft dynamics and control, because they provide a wider range of motion than other simulator technologies (for example, magnetic suspension systems), and offer a nearly torque-free environment as close as possible to that of space. Air-bearing simulators can be classified in two categories: planar systems and rotational systems. A rotational system allows for nearly unconstrained six degrees-of-freedom (dof) motion. A planar system, see Fig. 1, allows 2D translational motion and a single dof rotational motion. Planar systems have been used for orbital rendezvous problems, simulation of damaged satellite capturing, robot arm optimal joint trajectory to reduce vibration excitation within the arm elements, and autonomous extra-vehicular camera control law algorithm verification, [8].

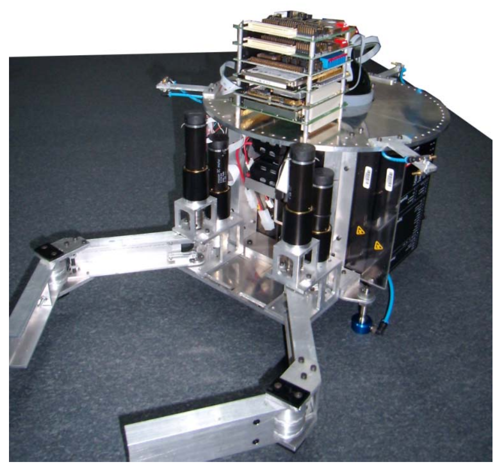

Figure 1. The NTUA air-bearing planar simulator robot.

In this paper, we address the problem of fuel minimization during point-to-point motions of an experimental air-bearing planar space robot. To achieve proportional control of 2-way on-off solenoid valves used for robot propulsion, a voltage PWM actuation is employed. The resulting thrust is analyzed, nonlinear valve effects are identified, and techniques tackling their shortcomings are proposed. The thruster behavior is used to design minimum fuel nozzle consumption strategies for point-to-point motions. A comparison between the thruster-only propulsion

Manuscript received October 16, 2006.

E. Papadopoulos is with the Department of Mechanical Engineering, National Technical University of Athens (NTUA), Greece (corresponding author, phone: +(30) 210-772-1440; fax: +(30) 210-772-1455; e-mail: egpapado@central.ntua.gr).

I. Kaliakatsos was with the Department of Mechanical Engineering, National Technical University of Athens, Greece (e-mail: ioannis.kaliakatsos@iris.mavt.ethz.ch). He is now with the Swiss Federal Institute of Technology (ETH Zurich), Institute of Robotics and Intelligent Systems.

D. Psarros was with the Department of Mechanical Engineering, National Technical University of Athens, Greece (e-mail: dpsarros@i-soft.gr).

ISBN: 978-960-89028-5-5

method with one including a reaction wheel is presented. A control algorithm for the simultaneous employment of thrusters and reaction wheel is proposed. It is found that under certain assumptions, the use of a reaction wheel further minimizes fuel consumption, increasing the useful life of a space robot.

II. Design of the Robot's Propulsion System

The basic elements of the experimental space robotics setup include: (a) A 2.3m x 2.0m x 0.30m granite table, (b) a free-flying robot, see Fig. 1, that hovers over the table, using 3 air-bearings, (c) a monitoring and control system, which determines the robot motion and controls the robot.

The propulsion system is responsible for the translational and rotational motion of the robot on the motion plane. By defining the design thrust to be approximately 1 N, with a design total impulse to be 100 Ns, Fig. 2 suggests the use of a monopropellant propulsion system, [3].

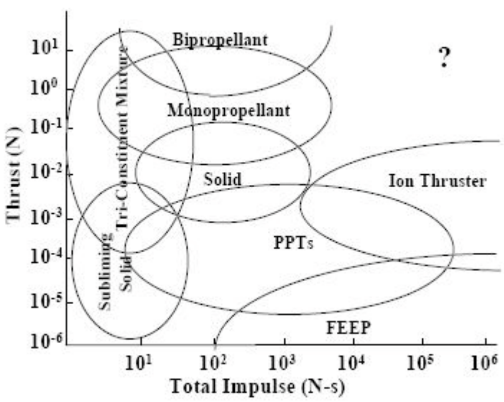

Figure 2. Operating range for potential thrust concepts, [3].

The choice of propellant is addressed next. The propellant must: (a) be available at low cost, (b) have a high ratio of "thrust/mass flow rate", (c) be stored in such a way, that long-term experiments are feasible, (d) not pose a threat to humans.

One option is hydrazine (N_2H_4), which is used in real space missions. However, hydrazine is toxic and cannot be used in the presence of humans, such as an Earth-based laboratory. Two other candidates are CO_2 and air. Air has higher "thrust/mass flow rate" ratio than CO_2, and is relatively free. However, its main disadvantage is its storage pressure. To fill a 20 oz. tank at 20° C, air must be stored at 200 bar, while CO_2 at 60 bar. Therefore, safety dictated the use of CO_2 as the propellant for our robot.

In the storage tank, CO_2 is in its two-phase region. Gaseous CO_2 leaves the tank whenever propulsion is needed, while the tank pressure is kept constant.

To control the thrust of the propulsion system, voltage-controlled solenoid valves were installed. Valves can be analog or on-off. In analog valves, the flow of the medium depends on valve actuation voltage. On the other hand, in on-off valves, the medium either flows or is totally blocked by the valve, independently of the voltage level application. On-off valves are essentially nonlinear, and thus more complex to control. However, analog valves cannot be used in actual space missions, since partial opening of the valve may result in solidification of the propulsion medium, and in blockage of the flow duct with a subsequent mission failure.

To design the space simulator as close as possible to space conditions, we use 6 normal-closed, 2-way, on-off, voltage actuated solenoid valves. To be able to approximate proportional actuation, a Pulse-Width-Modulation (PWM) scheme was designed, see Fig. 3. Since the valves need the CO_2 at 7 bar, a pressure regulator set at 7 bar was installed after the tank. The valves feed three counter-facing pairs of nozzles placed at 120° apart on the robot. There is no need to install additional nozzles and valves, since this does not improve robot controllability, while it increases fuel consumption. Installing fewer nozzles makes the robot less controllable. However, for redundancy reasons, two additional valves can be installed if future needs dictate so.

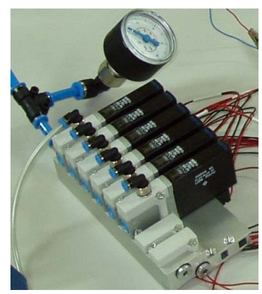

Figure 3. 2-way normal-closed, on-off solenoid valves on their manifold.

Although thrusters are necessary for translation, rotations can be achieved using an electric motor driven reaction wheel. This has the advantage of not using scarce fuel for applying torques, and will be discussed later in conjunction to thrusters.

III. Identification of Valve Behavior

As mentioned in the previous section, the on-off valves are actuated based on a voltage PWM scheme. In order to determine the thrust that can be obtained from each nozzle under this actuation scheme, we use the experimental setup shown in Fig. 4. As shown in this figure, a filter (A) is used for CO_2 filtering prior to its entrance in the manifold (E). When a valve is activated by the valve activation circuit (B), CO_2 flows through the valve to the nozzle, which is supported on a force sensor (F). A DAQ card (G) with additional force sensor signal conditioning (H) reads the value of thrust. A PWM signal generator (C) and a power supply (D) are also used. A close look-up of the valve activation circuit and the nozzle on the force sensor are shown in Fig. 5A and Fig. 5B respectively.

The activation circuit, see Fig. 5A, is designed to receive a logic input for each valve, and outputs a signal of the same waveform as the input, on a wider voltage scale (0-24 V), using the L293D IC chip.

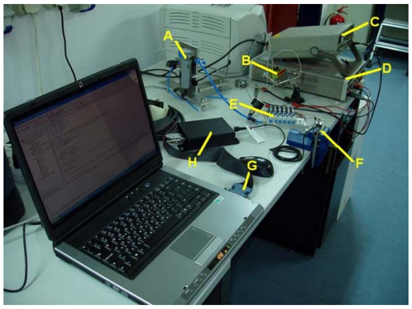

Figure 4. Experimental setup for determining nozzle thrust.

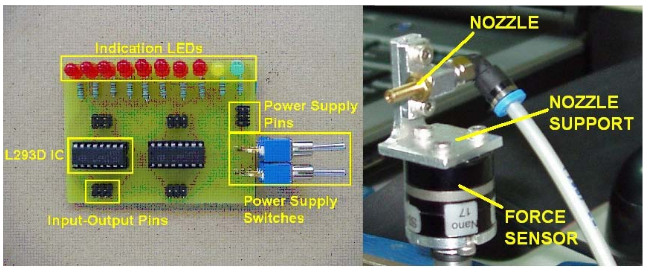

A B

Figure 5. A. Solenoid valve activation circuit. B. Thrust nozzle on an ATI nano force sensor.

Two power supply switches, which isolate the entire circuit from external power sources, are installed for safety reasons. Indication LEDs are also installed for debugging and to flash when the corresponding valve is signaled "on". It is apparent that the PWM input from the signal generator triggers the solenoid valves, which follow an activation pattern dictated by the main characteristic of the PWM, i.e. the duty cycle. The maximum frequency the valves can receive is 50 *Hz*, the nozzle has a constant diameter of 1.3 *mm* and is 6 *mm* long.

Our main goal here is to find a relationship between the thrust obtained and the PWM activation duty cycle. To this end, a number of experiments were run, each at a different duty cycle covering the entire range 0-100%, measuring the resulting thrust. The PWM carrier frequency was also varied in a range 5-50 *Hz.* The thrust values were averaged over 4 sample to minimize noise, and the mean value sampling frequency was 4.13 *kHz*. Each experiment was repeated three times for increased accuracy.

Fig. 6 plots the experimentally obtained nozzle thrust as a function of PWM duty cycle for a PWM carrier frequency of 20 *Hz*. It is clear from this figure that although for most of the duty cycle the thrust is proportional to it, a saturation region shows up relatively low on the duty cycle range (75%). This is related to the valve response time, which is 7*ms*. The "off" portion of the signal does not last long enough for the valve to follow. The void in experimental data shown in Fig. 6 between 0% - 20% and 80% - 99% duty cycle is due to the lack of experiments in these regions.

In our attempt to minimize the saturation region, we decided to decrease the activation carrier frequency. By reducing the activation frequency, the nonlinear regions in Fig. 6 are shortened. Fig. 7 shows relationship between thrust and duty cycle for a 7 *Hz* frequency.

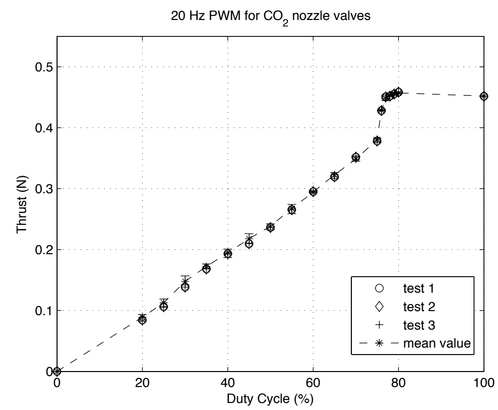

Figure 6. Thrust vs. valve activation duty cycle at 20 *Hz*.

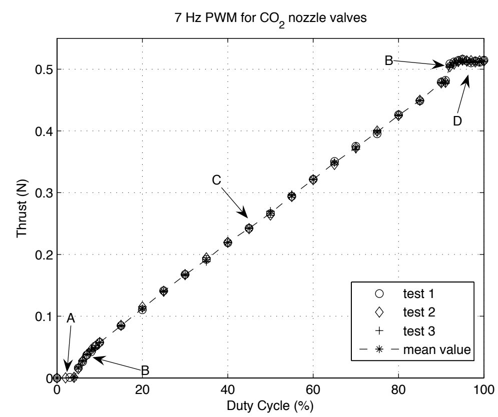

Figure 7. Thrust vs. valve activation duty cycle at 7 *Hz*.

Based on this figure, we make the following remarks: There is a wider linear region (C), which spreads from 10% to 90%. This means that the fluid system, which comprises of the valve, the CO_2 and the nozzle, behaves in a similar manner as does an electric motor when it is supplied with PWM voltage input. Also, there exists a dead-band region (A) which spreads from 0% to approximately 5%. This is again due to the valve response time, which does not allow for fast activation and de-activation of the valve. A saturation region (D) exists which spreads from approximately 93% to 100%. The adjustment between nonlinear regions A and D to the linear one (C) is made through the adjustment regions B.

It is clear that the nonlinear regions are smaller than in Fig. 6. One could further reduce the activation frequency in order to eliminate the non linear regions, but this would lead to a non uniform application of thrust and non modeled robot dynamics excitation. The fact that the maximum thrust for 20 *Hz* activation frequency (0.46 N) is less than that achieved for 7 *Hz* activation frequency (0.52 N), is due to CO_2 tank pressure present at the 20 *Hz* experiment (tank was not fully loaded).

IV. Nozzle Fuel Consumption Minimization

We examine next the minimum fuel consumption problem. The goal is to find the path that the robot should follow to move from an initial to a final configuration minimizing CO_2 consumption. To this end, a mathematical description of the robot behavior is needed. To simplify things in a initial study, we neglect one of the two manipulators and consider the other one as a single link arm, see Fig. 8.

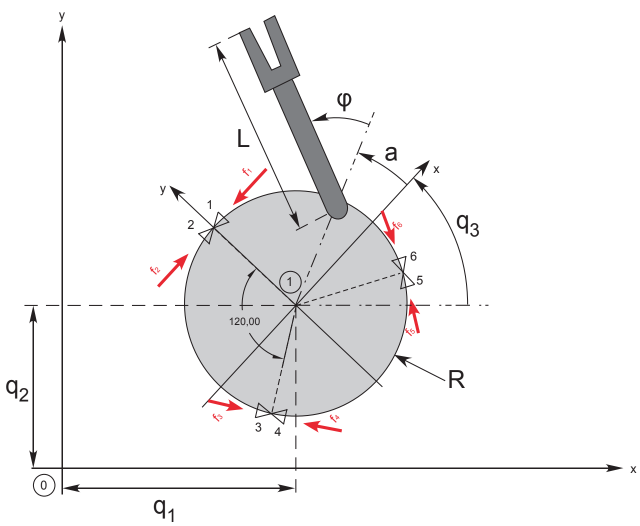

Figure 8. Robot planar motion description variables.

To derive a robot dynamics model, we use Lagrange equations. The governing equations of motion are:

$$\mathbf{M}(\mathbf{q})\ddot{\mathbf{q}}+\mathbf{C}(\mathbf{q},\dot{\mathbf{q}})\dot{\mathbf{q}}+\mathbf{V}(\varphi,\dot{\varphi},\ddot{\varphi})=\mathbf{R}_1^0(\mathbf{q})\mathbf{D}\mathbf{u} \tag{1}$$

$$\mathbf{q}=\begin{bmatrix}q_1 & q_2 & q_3\end{bmatrix}^T \tag{2}$$

$$\mathbf{u}=[f_1 \quad f_2 \quad \dots \quad f_6]^T \tag{3}$$

where q_i , $i=1,...,3$, are the robot coordinates shown in Fig. 8, φ is the arm angle, $\mathbf{q}$ is the robot vector, $\mathbf{M}(\mathbf{q})$ is the inertia matrix, $\mathbf{C}(\mathbf{q},\dot{\mathbf{q}})$ is the Coriolis and centrifugal matrix, $\mathbf{V}(\varphi,\dot{\varphi},\ddot{\varphi})$ is a vector representing the effect of arm motion, considered known, $\mathbf{R}_1^0(\mathbf{q})$ is the rotation matrix from the robot-fixed frame "1" to the inertial frame "0", $\mathbf{D}$ is the matrix that transforms the nozzle thrust vector into forces in axes x and y and torque about axis z, $\mathbf{u}$ is the nozzle thrust vector, and f_i , $i=1,...,6$, is the unilateral thrust from each nozzle expressed in reference frame "1". Matrices $\mathbf{M}(\mathbf{q})$, $\mathbf{C}(\mathbf{q},\dot{\mathbf{q}})$, $\mathbf{D}$ and vector $\mathbf{V}(\varphi,\dot{\varphi},\ddot{\varphi})$ are given in Appendix A. R is the radius of the cylindrical robot base, and L is the arm length.

Minimizing fuel consumption can be achieved following different methods, one of which is the use of generating functions and Hamiltonian Dynamics, [6]. While this method is mathematically solid, it is not straightforward to apply to nonlinear systems. Optimal Control is more suitable for nonlinear systems, and easier to program; hence it is employed here, see also Appendix B.

According to optimal control, the mathematical description of the minimization problem can be stated as follows. For given initial and final robot vectors:

$$\mathbf{q}_o = given, \quad \mathbf{q}_f = given \tag{4}$$

and given the manipulator motion:

$$\varphi=\varphi(t) \tag{5}$$

find the path the robot must follow in order to minimize CO_2 consumption by the nozzles, defined by the integral:

$$\text{consumption}=\frac{1}{2}\int_0^{t_f}\left(\mathbf{u}^T\mathbf{u}\right)dt \tag{6}$$

The robot dynamics are described by (1), which after manipulation can be written in the form:

$$\mathbf{z}_1=\mathbf{q}\ ,\ \mathbf{z}_2=\dot{\mathbf{q}}\ ,\ \mathbf{z}=\begin{bmatrix}\mathbf{z}_1^T & \mathbf{z}_2^T\end{bmatrix}^T$$

$$\dot{\mathbf{z}}=\begin{bmatrix}\mathbf{z}_2\\ \mathbf{M}(\mathbf{z}_1)^{-1}\left(-\mathbf{C}(\mathbf{z}_1,\mathbf{z}_2)\mathbf{z}_2-\mathbf{V}(\varphi,\dot{\varphi},\ddot{\varphi})+\mathbf{R}_1^0(\mathbf{z}_1)\mathbf{D}\mathbf{u}\right)\end{bmatrix} \tag{7}$$

Matrix $\mathbf{M}^{-1}$ always exists, since the inertia matrix is positive definite. Thus, the performance index becomes:

$$J=\gamma t_f+\frac{1}{2}\int_0^{t_f}\mathbf{u}^T\mathbf{u}dt \Rightarrow L=\frac{1}{2}\mathbf{u}^T\mathbf{u},\ \ S=\gamma t_f \tag{8}$$

where γ is a weighting factor between control time and control fuel consumption. The performance index is used in conjuction to (45) – (47), given in Appendix B, where the solving algorithm is also given. The algorithm convergence is checked upon by means of the following function:

$$\min_{\mathbf{h}} F(\mathbf{h})=\log\left(\sum_{i=1}^{n}\left|\hat{k}_i-k_i\right|\right) \tag{9}$$

where $\mathbf{h}=[\boldsymbol{\lambda}_0^T \quad t_f]^T$ is the design vector, k_i is the i^{th} boundary condition applied at t_f, and $\hat{k}_i$ is the i^{th} boundary condition estimated at t_f by the solution algorithm. Care should be taken so that the algorithm is not entrapped in a local minimum, or give a solution with no physical meaning (for example $t_f<0$). For this reason, we run the algorithm a number of times, each time starting from a different initial design vector guess. To implement the above, we use the MATLAB© subroutine "fminsearch," which is based on the Simplex algorithm.

In (9), the log function was chosen, because for either extremely large or extremely low arguments, it returns a result having reduced order of magnitude. Thus, it is computationally easier to incorporate in an algorithm in which the value of the objective function is large in the initialization phase and low near the completion of the algorithm.

V. Example

In this section we present an application example of the methodology presented earlier. Based on the previously described experiments and the results in Fig. 7, we may model the thrust as obeying the following inequality constraints:

$$f_{\min} = 0N \le f_i \le f_{\max} = 0.52N, \quad i = 1,\ldots,6 \tag{10}$$

For simulation purposes, the data given in Table I is used.

TABLE I

ROBOT GEOMETRICAL AND PHYSICAL DATA

Robot mass m_R [kg]	15.00	Arm mass m_L [kg]	0.20
Robot base radius R [m]	0.15	Arm length L [m]	0.30
Weighting factor	$\gamma = 1$	Angle a (Fig. 10) [deg]	$\pi / 6$

The initial and final robot vectors, as well as the desired arm motion, are given as:

$$\begin{aligned} \mathbf{q}_o &= [0 \quad 0 \quad 0]^T \\ \dot{\mathbf{q}}_o &= [0 \quad 0 \quad 0]^T \end{aligned} \tag{11}$$

$$\begin{aligned} \mathbf{q}_f &= [0.5 \quad 1 \quad -\pi/2]^T \\ \dot{\mathbf{q}}_f &= [0 \quad 0 \quad 0]^T \end{aligned} \tag{12}$$

$$\begin{aligned} \varphi_o &= \pi/3 \\ \varphi_f &= -\pi/2 \end{aligned} \tag{13}$$

$$\varphi(t) = \varphi_o + 3(\varphi_f - \varphi_o)\left(\frac{t}{t_f}\right)^2 - 2(\varphi_f - \varphi_o)\left(\frac{t}{t_f}\right)^3 \tag{14}$$

The solution for the Lagrange multipliers vector, (see Appendix B), is found to be:

$$\boldsymbol{\lambda}_0 = [-0.425 \; -0.857 \; 0.005 \; -2.751 \; -5.525 \; 0.028]^T \tag{15}$$

and the final trajectory time is:

$$t_f = 13.16 \text{ s} \tag{16}$$

Fig. 9 shows snapshots from the resulting fuel-optimal path and the corresponding orientation history. The robot base seems to follow a straight path between the initial and final position. This is due to the low mass of the arm (0.2 kg) compared to the mass of the robot base (15 kg), since here, the manipulator nonlinearity has a small effect.

The configuration variables q_1, q_2 and q_3 are shown in Fig. 10, while the desired arm motion is shown in Fig. 11. The thrust from each nozzle is shown in Fig. 12. Only 2.90% of the full tank (20 oz ≈ 540 g) is used, which is low.

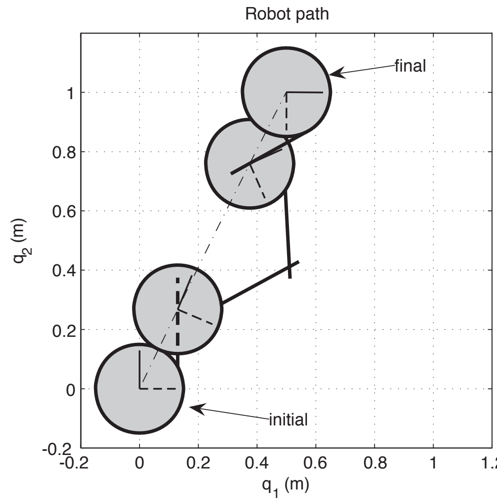

Figure 9. Snapshots of optimal robot path.

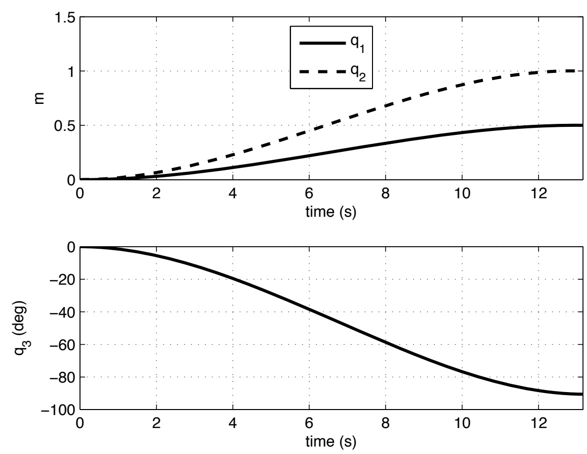

Figure 10. (a) Detail of variables q_1 and q_2, (b) Detail of q_3 (robot orientation).

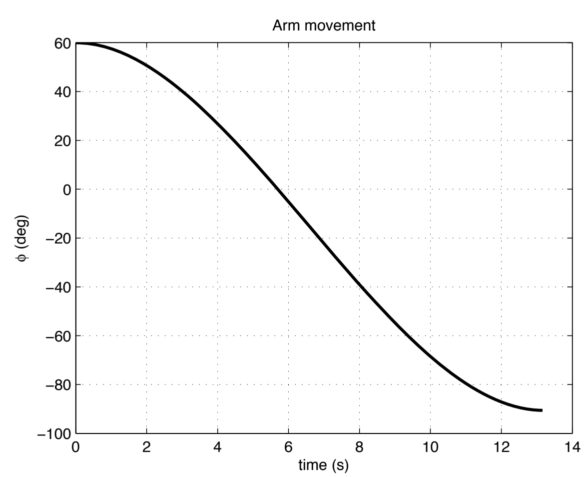

Figure 11. Desired arm motion.

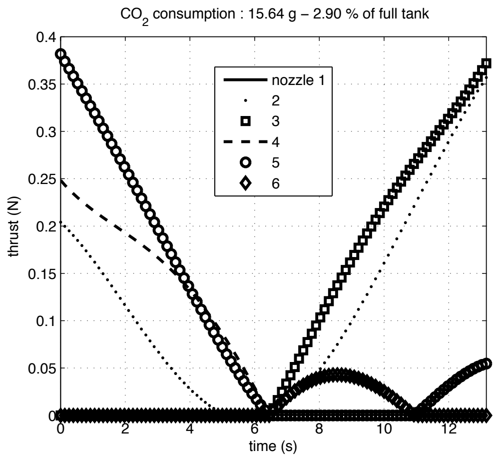

Figure 12. Individual nozzle thrust and total CO_2 consumption.

VI. Alternative Approach Using a Reaction Wheel

A reaction wheel is a momentum exchange device, used for spacecraft attitude control. Its operation is based on the conservation of angular momentum and is electrically powered. Using this device allows one to avoid the use of thrusters for the production of a torque vector.

Although in the case of thruster-only actuation, one can minimize fuel use with appropriate algorithms as was done in the previous section, it is inevitable that some of the thrust generated by one actuator is counterattacked by the thrust produced by another. Mathematically speaking, this is due to the existence of a null space in matrix **D**. It is obvious that the minimum consumption will be attained if one can use the full thrust of a nozzle to accelerate the robot only. This is possible if a reaction wheel is used. The idea is to generate a force by activating a thruster acting parallel to the desired force direction, while the reaction wheel counteracts any unwanted torque. This is illustrated in Fig. 13A. On the top figure, the horizontal components of the thruster force do not contribute to accelerate the robot base.

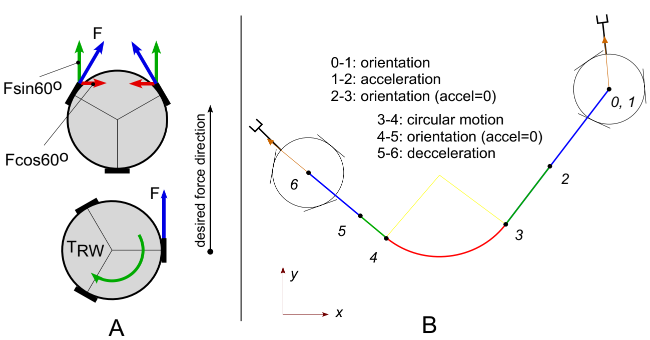

Figure 13. A: Force generation methods. B. Reference trajectory for comparisons.

However, when the reaction wheel is activated, a single thruster accelerates the base without any loss of fuel, while the torque needed to avoid base rotations is provided by the wheel. In addition, if a pure rotation is needed, then no thrusters need to be activated.

Next, we compare the two actuation methods, i.e. using thrusters only and using thrusters with a wheel. A planar trajectory was developed that can be used in both cases and that can provide obstacle avoiding capabilities. The path consists of two straight lines and a circular sector, and is shown in Fig. 13B.

In each case, appropriate constraints such as thruster force limits or torque-speed characteristics are taken into account. Since reaction wheels can saturate, i.e. not be able to produce more torque due to their high rotational speed, then, appropriate thrusters must be activated to produce the torque difference. This is shown in Fig. 14, where the control software checks the condition of the reaction wheel, and if no additional torque can be supplied, the thrusters are turned on. The appearance of saturation depends on the size of the motor and flywheel. The reaction wheel employed is designed such that the wheel at its nominal rpm can supply a torque required to re-orient the robot at reasonable time. Motor saturation may still occur, when high angular accelerations at the presence of high rpm, are needed. In general, a flywheel of large inertia reduces this probability.

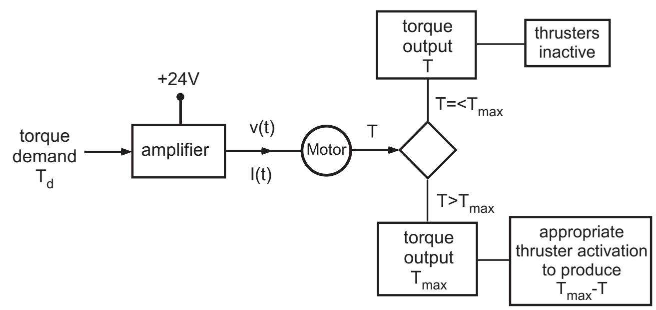

Figure 14. Attitude and propulsion system interaction.

The total thrust is given by,

$$\text{total thrust} = k \cdot \sum_{i=1}^{6} \int_{0}^{t_f} f_i(t)\,dt \tag{17}$$

where k is a constant. The developed thrust is considered as the appropriate criterion for evaluating the two cases. After simulating robot motion in both cases, it was found that the results were superior when using a reaction wheel. As shown in Figs. 15 and 16, the reduction in CO_2 consumption can be over 50%.

As expected, higher thruster forces appear during translational motion with accelerations, while almost no thruster activation occurred during the combined motion (translation and rotation without acceleration), when a reaction wheel is employed. In Fig. 15, one may also notice the simultaneous activation of two thrusters during translations, while in Fig. 16, only the nozzle that parallel to the desired direction, is activated.

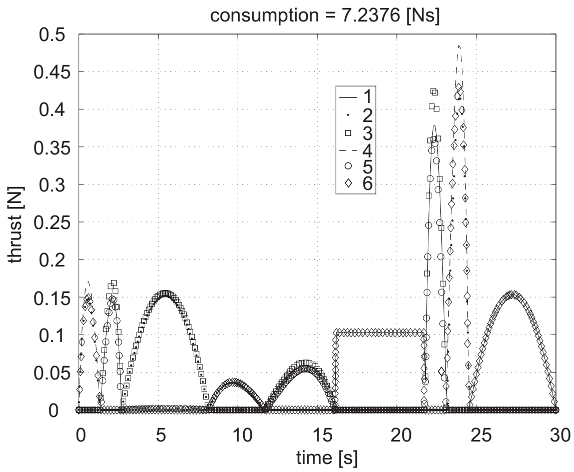

Figure 15. Thruster forces without using reaction wheel.

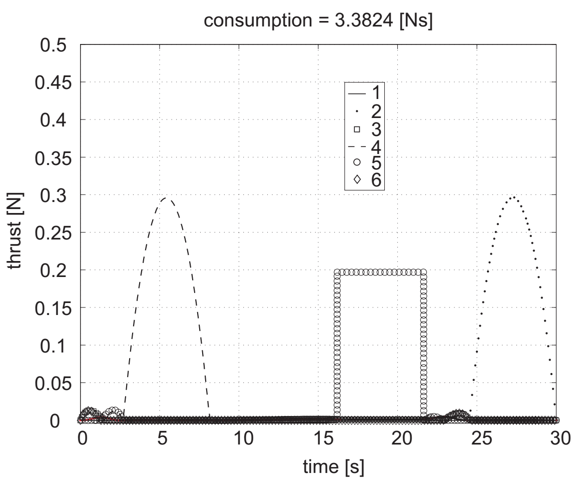

Figure 16. Thruster forces using a reaction wheel.

However, a drawback of using the single nozzle-wheel methodology is that the maximum total force that can be applied to the base is the maximum force, $F_{\max}$, that a single thruster can generate. On the contrary, if only thrusters are used, the maximum force is equal to $\sqrt{3}F_{\max}$. Therefore, if maximum acceleration is needed, then some fuel will be spent without getting useful acceleration from it.

In conclusion, the use of a reaction wheel improves robot performance, under the fuel consumption criterion. Trajectory has to be designed and optimized for the specific case of motion, considering all limitations. A significant increase of consumption may occur during motor saturation, depending on its specifications and robot torque demand.

VII. Conclusions

A planar air-bearing space robot simulator has been developed. Its propulsion system uses CO_2 and solenoid valves controlled by voltage PWM. The thrust obtained by this activation was mostly linear, and narrow non-linear regions arose due to high valve response time. Non-linear regions expanded and the linear one shrank, when the input PWM signal frequency increased. Thus the PWM frequency was kept relatively low at 7 *Hz* compared to the valve's maximum attainable input frequency of 50 *Hz* To minimize nozzle fuel optimal control theory, with thrust inequality constraints was used. The effect of using a reaction wheel was investigated aiming at additional reduction of CO_2 consumption. A control algorithm for the simultaneous employment of thrusters and reaction wheel was designed and compared with the thrusters only case using a general path. It was found that under certain assumptions, the use of a reaction wheel further minimizes fuel consumption, increasing the useful life of a space robot.

VIII. Acknowledgements

Support by the EPAN Cooperation Program 4.3.6.1.b (Greece-USA 035) of the Hellenic General Secretariat for Research and Technology is acknowledged.

References

[1] Bryson A.E. Jr., Ho Y., *Applied Optimal Control*, Revised Printing, Taylor & Francis, 1975.

[2] Cardin M.J., Acosta J., "Design and test of an economical cold gas propulsion system", *14th Annual/USU Conference on Small Satellites,* 2000.

[3] Groot W.A., "Propulsion Options for Primary Thrust and Attitude Control for Microspacecraft", *NASA/CR-1998-206608,* March, 1998.

[4] Martin E., Papadopoulos E., Angeles J., "Towards Reducing Thruster-Flexibility Interactions in Space Robots", *Proc. of the 11th CISM-IFToMM Symposium on Theory and Practice of Robots and Manipulators*, July 1-4, 1996, Udine, Italy.

[5] Menon, C., Busolo, S., Cocuzza, S., Aboudan, A., Bulgarelli, A., Bettanini, C., Angrilli, F., "Issues and new solutions for testing free-flying robots", *IAC-04-IAF-1.J.5,* 2004.

[6] Park C., Scheeres D.J., "Solutions of the Optimal Feedback Control Problem using Hamiltonian Dynamics and Generating Functions", *Proc. 42nd IEEE Conference on Decision and Control,* Paper TuP07.3, Maui, 2003.

[7] Robertson M.J., Singhose, W.E., "Deflection-Limiting Control of Flexible Spacecraft Using On-Off Thrusters," *University Space Systems Symposium*, Honolulu, HI, 2002.

[8] Schwartz J.L., Peck M.A., Hall C.D., "Historical Review of Air-Bearing Spacecraft Simulators", *Journal of Guidance, Control and Dynamics,* Vol. 26, No. 4, July-August, 2003.

Appendix A - Dynamics Model Matrix Elements

The elements of matrix $\mathbf{M}(\mathbf{q})$ are given by,

$$m_{11} = m_L + m_R \tag{18}$$

$$m_{12} = 0 \tag{19}$$

$$m_{13} = -m_L\left[R\sin(a+q_3)+\frac{1}{2}L\sin(a+q_3+\varphi)\right] \tag{20}$$

$$m_{21} = 0 \tag{21}$$

$$m_{22} = m_L + m_R \tag{22}$$

$$m_{23} = m_L\left[R\cos(a+q_3)+\frac{1}{2}L\cos(a+q_3+\varphi)\right] \tag{23}$$

$$m_{31} = -m_L \left[R\sin(a+q_3) + \frac{1}{2} L\sin(a+q_3+\varphi) \right] \tag{24}$$

$$m_{32} = m_L \left[R\cos(a+q_3) + \frac{1}{2} L\cos(a+q_3+\varphi) \right] \tag{25}$$

$$m_{33} = I_R + I_L + m_L LR\cos\varphi + m_L \left(R^2 + \frac{L^2}{4} \right) \tag{26}$$

The elements of matrix $\mathbf{C}(\mathbf{q},\dot{\mathbf{q}})$ are given by,

$$c_{11} = 0 \tag{27}$$

$$c_{12} = 0 \tag{28}$$

$$c_{13} = -\dot{q}_3 m_L \left[R\cos(a+q_3) + \frac{1}{2} L\cos(a+q_3+\varphi) \right] - -\dot{\varphi} m_L L\cos(a+q_3+\varphi) \tag{29}$$

$$c_{21} = 0 \tag{30}$$

$$c_{22} = 0 \tag{31}$$

$$c_{23} = -\dot{q}_3 m_L \left[R\sin(a+q_3) + \frac{1}{2} L\sin(a+q_3+\varphi) \right] - -\dot{\varphi} m_L L\sin(a+q_3+\varphi) \tag{32}$$

$$c_{31} = 0 \tag{33}$$

$$c_{32} = 0 \tag{34}$$

$$c_{33} = -\dot{\varphi} m_L LR\sin\varphi \tag{35}$$

Based on the selected symmetrical placement of thrusters, the matrix $\mathbf{D}$ is,

$$\mathbf{D} = \begin{bmatrix} -1 & 1 & \frac{1}{2} & -\frac{1}{2} & \frac{1}{2} & -\frac{1}{2} \\ 0 & 0 & -\frac{\sqrt{3}}{2} & \frac{\sqrt{3}}{2} & \frac{\sqrt{3}}{2} & -\frac{\sqrt{3}}{2} \\ R & -R & R & -R & R & -R \end{bmatrix} \tag{36}$$

Finally, the elements of the vector $\mathbf{V}(\varphi,\dot{\varphi},\ddot{\varphi})$ are:

$$v_{11} = -\dot{\varphi}^2 \frac{1}{2} m_L L\cos(a+q_3+\varphi) - \ddot{\varphi} \frac{1}{2} m_L L\sin(a+q_3+\varphi) \tag{37}$$

$$v_{21} = \frac{m_L L}{2} \left[-\dot{\varphi}^2 \sin(a+q_3+\varphi) + \ddot{\varphi}\cos(a+q_3+\varphi) \right] \tag{38}$$

$$v_{31} = -\dot{\varphi}^2 \frac{m_L L}{2} R\sin\varphi + \ddot{\varphi} \left(I_L + \frac{m_L L}{2} R\cos\varphi + \frac{m_L L^2}{4} \right) \tag{39}$$

APPENDIX B - OPTIMAL CONTROL

Let a system be subject to the following system equations:

$$\dot{\mathbf{x}} = \mathbf{f}(\mathbf{x},\mathbf{u},t) \tag{40}$$

where vector $\mathbf{x} = \mathbf{x}(t) \in \mathbb{R}^n$ is the state vector of the system, vector $\mathbf{u} = \mathbf{u}(t) \in \mathbb{R}^m$ is the control vector, t is time, and function $\mathbf{f} \in \mathbb{R}^n$ is a vector function, nonlinear in the general case.

Let the performance of the system be judged upon by the value of a performance index, having the form:

$$J = S(t_f) + \int_{t_0}^{t_f} L(\mathbf{x},\mathbf{u},t)\,dt \tag{41}$$

where $S(t_f)$ is a scalar function of the final control time t_f. Let, also, the control vector be subject to the following inequality constraints:

$$c_i(\mathbf{u},t) \le 0 \quad , \quad i = 1,...,\kappa \tag{42}$$

Thus, finding the optimal value of (41) can be mathematically stated as: "Find the control vector $\mathbf{u} = \mathbf{u}(t) \in \mathbb{R}^m$, subject to constraints (42), which minimizes (41) for the system (40)."

The solution to the above problem is found by defining the following scalar functions:

$$H^o = L + \boldsymbol{\lambda}^T \mathbf{f} \tag{43}$$

and

$$H = L + \boldsymbol{\lambda}^T \mathbf{f} + \boldsymbol{\mu}^T \mathbf{C} \tag{44}$$

where vector $\boldsymbol{\lambda} = \boldsymbol{\lambda}(t) \in \mathbb{R}^n$ is the Lagrange multipliers vector for the system dynamic equations, vector $\boldsymbol{\mu} = \boldsymbol{\mu}(t) \in \mathbb{R}^\kappa$ is the Lagrange multipliers vector for the control law inequality constraints, and vector $\mathbf{C} = [c_1, \ c_2, \ ..., \ c_\kappa]^T$ is the vector of control law inequality constraints. It can be shown that the following conditions are sufficient for the solution to hold, [1]:

$$\frac{\partial H}{\partial \mathbf{u}} = 0, \quad \text{where } \mu_i \begin{cases} \ge 0, c_i = 0 \\ = 0, c_i < 0 \end{cases} \tag{45}$$

$$\dot{\boldsymbol{\lambda}} = -\frac{\partial H^o}{\partial \mathbf{x}}, \quad \dot{\mathbf{x}} = \mathbf{f}(\mathbf{x},\mathbf{u},t) = \frac{\partial H^o}{\partial \boldsymbol{\lambda}} \tag{46}$$

$$\mathbf{x}(t_o) = given, \quad \mathbf{x}(t_f) = given, \quad \left(\frac{\partial S}{\partial t_f} + H^o \right)_{t=t_f} = 0 \tag{47}$$

It should be noted that final control time t_f is an unknown to be determined by (47). As can be noticed from (46)-(47), the above problem is a first order, two-point boundary value problem: one specifies $\mathbf{x}$ at time $t = t_o$ and $t = t_f$, but leaves $\boldsymbol{\lambda}$ to be determined so that the above holds. The solution algorithm we follow can be briefly stated as:

- Assume initial values for $\boldsymbol{\lambda}(t = t_o) = \boldsymbol{\lambda}_0$ and t_f.
- Integrate (46) from t_o to t_f. The control vector is to be found from (45).
- Check boundary conditions (47). If not matched, change the initial assumptions $\boldsymbol{\lambda}(t = t_o) = \boldsymbol{\lambda}_0$, and t_f, until convergence occurs.